Role of Nanoscale Crystallinity on the Recovery of Rare Earth Elements (REEs) from Coal Fly Ash

Sheila Gerardo, Kevin Matthews, Jamie Warner, and Wen Song*

Cite This: *Environ. Sci. Technol. Lett.* 2023, 10, 943–948
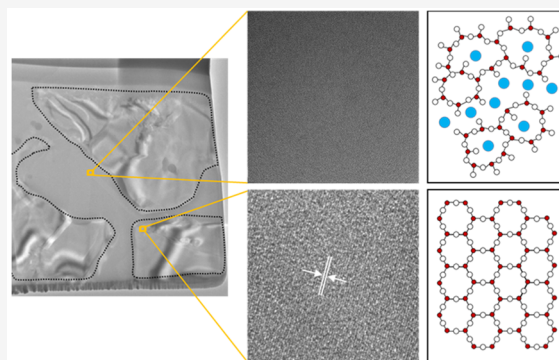
Read Online

ACCESS | Metrics & More | Article Recommendations | Supporting Information

ABSTRACT: Reclamation of coal fly ash, a legacy waste material, provides an alternative pathway for the recovery of rare earth elements (REEs) while reducing the environmental stresses that stem from traditional mining. The reactive transport processes underlying the recovery of REEs from ash wastes, however, are yet to be fully elucidated owing to the physicochemical complexity of the micro/nanoscale fly ash particles, including the crystallinity of the particulate matrix. In this work, we use transmission electron microscopy to characterize the material properties of ash particles and reveal the impact of crystallinity on the reactive transport processes governing access to and recovery of the encapsulated REEs. Our results show, for the first time, two distinct crystalline structures of REE-bearing aluminosilicate particles: dense amorphous matrices that facilitate the exchange of chemical species through their lattice interstices and porous polycrystalline matrices characterized by connected intraparticle pores and chemical inertness to leaching solutions. Notably, the presence of matrix crystallinity, or the lack thereof, governs the extent of reagents consumed parasitically by secondary reactions with the aluminosilicate matrix. Our work reveals how the variability of crystalline structures of the ash matrices hosting REEs defines the pathways for the recovery of REEs, providing key insights required for the development of targeted recovery processes.

KEYWORDS: *rare earth elements, crystallinity, CFA, remediation, reactive transport mechanisms*

1. INTRODUCTION

Climate change mitigation requires unprecedented quantities of rare earth elements (REEs) critical for the at-scale manufacturing of low-carbon technologies.[1−5] The current sourcing of REEs, however, relies on traditional mining activities that lead to land clearing, release metal contaminants into the soil, and emit high levels of carbon dioxide.[6−8] For instance, some of the world's largest deposits of REEs are dominated by carbonatite minerals that, when exposed to hydrometallurgical processes, release CO_2 and fluorine-bearing gases.[9,10] An alternative approach to conventional mining for the recovery of REEs is to repurpose fly ash, a coal combustion legacy waste, that contains increased concentrations of REEs.[11,12] Importantly, reclaiming fly ash disposed of in surface facilities enables direct access to the resource, minimizes open-pit mining of REEs, and reduces the risk of leakage of ash[13,14] into local ecosystems.

Current approaches[15,16] for the recovery of REEs from fly ash, however, are challenged by our limited understanding of the fundamental particulate material properties and reactive transport processes. While previous studies show that REE-bearing minerals are found primarily encapsulated in microscopic aluminosilicate particles (∼20 μm), these particulates are highly heterogeneous in composition and physical characteristics.[17−21] Importantly, ash particulates can be categorized broadly by their internal morphology as having either solid (hereafter "dense") matrices with no internal porosity or those with interconnected pores (hereafter "porous" matrices) that enable intraparticle flow.[22] Distinct transport and reactive phenomena therefore take place at the subparticle level during the recovery of REEs. Acid leaching [e.g., hydrochloric acid (HCl) and nitric acid (HNO_3)], in particular, recovers up to ∼60% of total REEs from the dense particles with noticeable metals leached (Al, Mg, Ca, Na, and K) from the solid matrix, while porous particles yielded high recoveries of REEs (>90%) without compositional or physical changes.[22] Such stark differences in matrix reactivities between the dense and porous aluminosilicate particles reveal that elemental composition and intrinsic porosity alone do not fully elucidate the phenomena that take place and underscore the

need to investigate additional characteristics of the particle matrix.

Crystallinity is a fundamental property that impacts the reactivity and ion diffusivity of the material phases. Aluminosilicates with similar compositions but different crystal structures, for example, present distinct dissolution rates and mechanisms.[23−25] A thorough understanding of the processes that govern the recovery of REEs therefore requires the characterization of the crystal structures of the ash matrices that encapsulate REE-bearing minerals. Although bulk techniques such as X-ray diffraction (XRD) and sequential extraction have been used to investigate the crystallinity of bulk ash composites,[17,26] these methods lack the spatial resolution required to elucidate the particle- and subparticle-level heterogeneities. In this study, we investigate the crystal structures of REE-hosting ash matrices via transmission electron microscopy (TEM) and elucidate their role in the accessibility and recovery of REEs. While previous TEM studies[27,28] have investigated the nanoscale occurrences of the REE minerals in ash, understanding of the crystallographic characteristics of the embedding ash matrix is still lacking. The results presented here reveal the presence of distinct crystalline structures prevalent in dense and porous particles, and we discuss their impact on cation transport and REE-bearing mineral dissolution. On the basis of the crystallographic, elemental, and morphologic characteristics of the ash particles, we propose mechanisms here to explain the reactive transport differences in dense and porous particles observed during the recovery of REEs. We further discuss the implications of the crystallinity, and lack thereof, of ash matrices on the leaching of secondary cations, providing relevant information for the development of methods for the extraction of environmentally benign REEs.

2. MATERIALS AND METHODS

A fly ash sample was collected from a power plant in Wyoming with a Powder River Basin coal feedstock (Table S1). The procured ash was mixed thoroughly to reduce preferential sampling of smaller fly ash particulates at the top of the container. Ash sample batches were then sieved through a No. 50 mesh (<300 μm) to remove clastic contaminants and stored in capped plastic containers prior to characterization and recovery analysis. No other treatment of the ash was performed. The bulk and microscale properties of this ash sample were reported previously.[22] In summary, the bulk mineralogy of the fly ash consists of amorphous aluminosilicate, quartz, hematite, mullite, and anhydrite.[22] The total content of REEs in this sample is 384 ± 32 ppm.[22] Microvisual characterization of milled ash particles shows that approximately 90% of REE-bearing minerals were encapsulated in the dense and porous matrix aluminosilicate particles; the remainder were either discrete or bound to the surface of ash particles and were directly accessible to leaching reagents.[22] Importantly, although our previous microvisual characterization work was performed in a two-dimensional plane, the large number of REE minerals analyzed (97 in total) and symmetry of the ash particles suggest full encapsulation in the unadulterated three-dimensional material.

The crystallinity of REE-bearing particles was investigated by using electron microscopy techniques (Figure 1A). Dense and porous ash particles containing REE minerals were identified in epoxy-mounted, argon ion-milled ash using scanning electron microscopy (SEM) [Scios 2 HiVac Dual-

Beam (Figure 1A and Figure S1)]. Thin lamellae were extracted from the matrix of the particles using a focused ion beam (FIB), attached to a lift-out grid, and further milled to a thickness of ∼100 nm. The lamellae were imaged using scanning transmission electron microscopy (STEM) (JEOL neoARM) in TEM and STEM modes at 200 keV. Annular dark-field (ADF) STEM imaging coupled with EDS was performed to evaluate the elemental composition of the matrix of the REE-hosting ash particles. High-resolution TEM (HRTEM) and fast Fourier transform (FFT) were used to investigate the crystallinity of the REE-bearing ash matrix lamellae. Matrix lattice characteristics (i.e., d spacing) were calculated from the FFT patterns using ImageJ.

3. RESULTS AND DISCUSSION

3.1. Dense Matrix Particles. STEM-EDS data reveal that the matrix of the dense particle consists primarily of an aluminosilicate phase with silicate fragments incorporated throughout (Figure 1B,C). Overlapping elemental maps of silicon, aluminum, and oxygen across the continuous phase suggest that the matrix is an aluminosilicate. The fragments, in contrast, are characterized by Si and O without aluminum signals, indicating that their composition consists of silicon oxide [i.e., silicate (Figure 1C)].

Notably, HRTEM crystallinity data of the dense matrix lamella showed two distinct phases: a continuous amorphous phase that coincides with the aluminosilicate material and crystalline regions coinciding with the silicate fragments (Figure 1). The crystallinities of the continuous aluminosilicate phase and of the silicate fragments were determined using three data sets: (i) the location and distribution of Fresnel fringes in HRTEM images, (ii) the presence, or lack, of lattice fringes in HRTEM, and (iii) the corresponding FFT patterns of the HRTEM data. First, Fresnel fringes, indicative of crystal boundaries and dislocations,[29] were observed across the silicate fragments but not in the continuous aluminosilicate phase (Figure 1B). Second, the absence of crystalline lattice fringes confirms that the aluminosilicate phase is amorphous (Figure 1D). Notably, the corresponding FFT shows only a halo and lacks distinct spot patterns, further corroborating the amorphous nature of the aluminosilicate phase. In contrast, HRTEM imaging of the silicate fragments exhibited lattice fringes that indicate periodic crystal lattices in the silicate phase (Figure 1E). Spot patterns are noticeable in the FFT data of the silicate fragments with a lattice d spacing of 2.2 Å (Figure 1E).

Amorphous phases found in fly ash present structural interstices (i.e., free volume within the lattice network) that enable the transport of chemical species and facilitate access to REEs encapsulated by dense matrices (Figure 2A). Specifically, variations in bond lengths and angles, rotated lattice units, as well as the incorporation of alkali and alkali earth metals, disrupt the lattice network and create ring structures that generate interstitial volume.[30,31] Metal cations (i.e., Na, K, Mg, and Ca) in the amorphous ash matrix are thus able to use the interstices to diffuse outwardly in exchange for protons that diffuse into the matrix of the particle. Moreover, while diffusion coefficients for ions through glassy matrices are relatively small (e.g., 10^{-8} to 10^{-10} cm^2/s in sodium−silicate glasses[32]), glass−fluid interactions in fly ash are bolstered by the large surface area of the microscopic ash particles (∼10 nm to 100 μm). Proton access to REEs encapsulated within dense matrix particles, therefore, does not require interconnected porosity
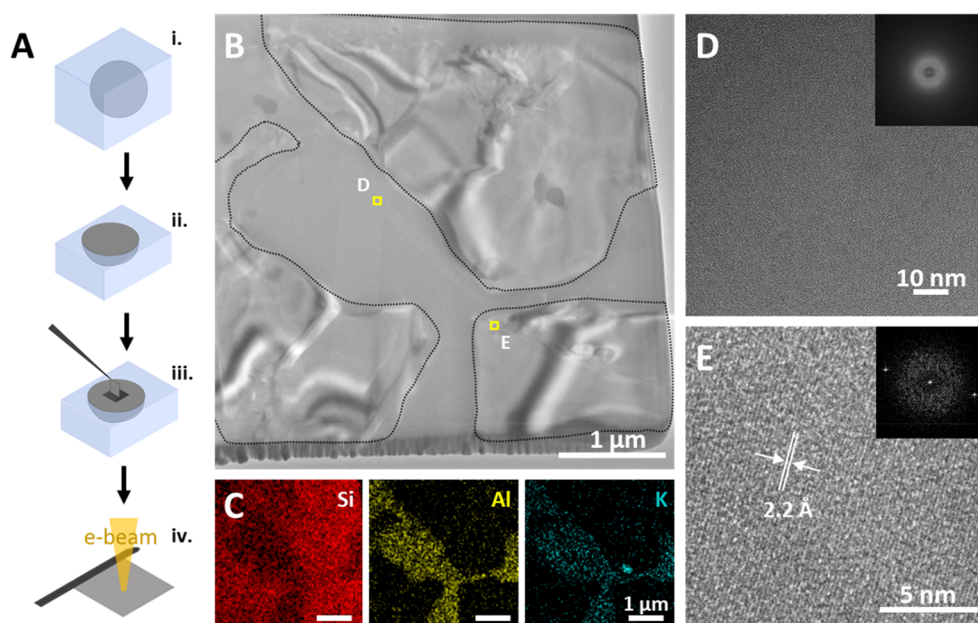
Figure 1. (A) Thin lamellae were extracted from ash particles by (i) preparing epoxy-mounted ash particles, (ii) argon ion milling the ash sample, (iii) sectioning off the lamellae from REE-bearing particles, and (iv) attaching the lamellae to a grid to enable the transfer of the sample to the transmission electron microscope. (B) HRTEM image of the lamella obtained from a dense matrix particle. Regions delimited by the black dashed line correspond to crystalline fragments incorporated in the matrix of the particle. The highlighted yellow boxes indicate where the TEM data shown in panels D and E were taken. (C) Corresponding EDS elemental maps of silicon, aluminum, and potassium show silicate fragments dispersed in an aluminosilicate continuous phase. (D) HRTEM image of the amorphous phase, showing no visible lattice fringes. The inset corresponds to the FFT image, showing only a halo and confirming that the aluminosilicate phase is amorphous. (E) HRTEM image of the silicate fragments, showing lattice fringes and distinct spots in the FFT image, corroborating the crystalline nature of the fragments.

but rather is enabled by the lattice interstices available in their amorphous phase. Leaching methods, however, generally lack selectivity and result in the indiscriminate release of cations, including non-REE species, from the amorphous matrix. A trade-off, therefore, exists in the recovery of REEs from dense amorphous particles, where the extraction of REEs is accompanied by contaminated solutions that require intensive separation downstream.

3.2. Porous Matrix Particles. STEM-EDS elemental data of the porous matrix showed a homogeneous aluminosilicate composition across the lamella (Figure S2). Increased concentrations of silicon and aluminum were detected throughout the matrix with a Si:Al ratio of 1:1, whereas alkali/alkali earth cations were found at only minor levels (Figure S2). The porous internal morphology and elemental composition of these particles (i.e., 1:1 Si:Al ratio) resemble those of calcined clay particles.[33,34] Both the top view of the porous particle slice and the side view revealed by the TEM lamella (Figure S1B,D) show that the REE minerals are surrounded by the ash matrix, indicating full encapsulation of REE minerals within the particle.

HRTEM characterization shows that the porous lamella was comprised of a polycrystalline matrix that consists of randomly oriented nanocrystals [∼10 to 100 nm (Figure 3)]. HRTEM data collected from the matrix showed distinctly oriented crystal grains across the matrix of the lamella, with *d* spacing values ranging from 1.3 to 5.5 Å (Figure 3A and Figures S3−S6). Importantly, textural heterogeneity across the lamella, indicative of spatial density variations, shows that the polycrystalline behavior extends across the entire matrix (Figure 3B,C and Figure S7). Ring patterns in the FFT data, with predominant *d* spacings of 3.5 and 5.5 Å, further

corroborate the existence of polycrystallinity in the porous matrix (inset of Figure 3C).

The crystalline nature of the porous particle matrices explains previous observations[22] of their unchanged composition throughout the recovery of REEs via leaching treatments. Crystalline aluminosilicates possess fewer interstices than their amorphous counterparts such that reactions with leaching solutions are primarily restricted to solid−fluid interfaces (as opposed to solid-state transport in the case of amorphous matrices).[23,25] Consequently, REE-bearing minerals in porous matrices are recovered via fluid transport through intraparticle pores, while the polycrystalline aluminosilicate matrix remains unaltered (Figure 2B). A potential advantage of the less reactive polycrystalline matrices is minimal depletion of reagents in parasitic reactions with the bulk ash matrix and, subsequently, reduced amounts of contaminants released into the leaching solution. Specifically, REEs recovered from crystalline porous matrices are expected to yield lower levels of secondary metals (e.g., Al, Ca, Mg, Na, and K) in the effluent solutions, reducing the separation requirements in downstream operations.

The potential for the lower reagent consumption and purer effluents suggests that ash samples with a greater degree of porosity and crystallinity may provide a more efficient path for the extraction of REEs. As discussed above, the physiochemical properties of porous ash particles suggest that they originate from clays and have maintained their crystalline structures as a result of limited exposure to combustion.[33,35] Amorphous matrices formed from the rapid solidification of molten minerals, on the contrary, result from firing at high temperatures. Coal combustion temperatures and residence times therefore could be adjusted to reduce the amorphous content generated in the ash to improve the the overall
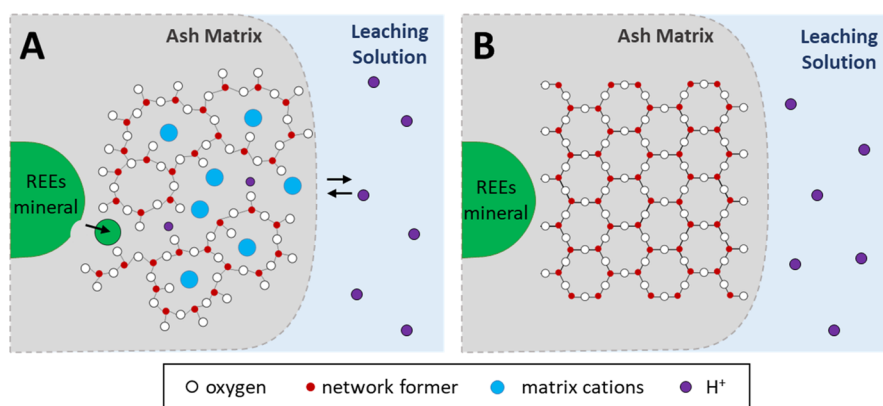
Figure 2. Mechanisms controlling the recovery of REE minerals (e.g., monazite, bastnaesite, and REE oxides) depend on the crystal structure of the encapsulating ash matrix. (A) Dense amorphous matrices enable cation exchange through lattice interstices, while (B) porous crystalline particles are more stable and consequently show greater resistance to leaching solutions. The atomic structures presented here are examples of amorphous and crystalline silicate atomic arrangements.[30,31] Network formers refer to Si, whereas matrix cations refer to incorporated metals, such as alkali metals.
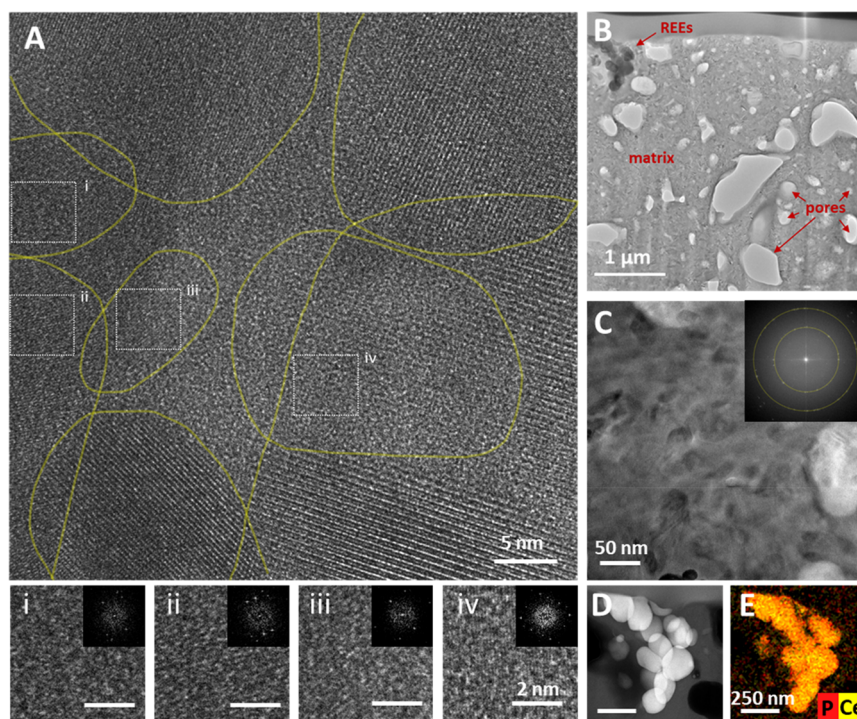

Figure 3. (A) HRTEM imaging of the porous matrix shows lattice fringes of randomly oriented grains, confirming the polycrystalline structure of the matrix. Crystal grains where lattice fringes are harder to distinguish are magnified in panels i–iv. (B) HRTEM image of the lamella showing a textured porous matrix, indicative of density variations across the material. (C) HRTEM image of the porous matrix collected at 120K× magnification, showing a textured matrix. The computed FFT pattern (inset) shows ring patterns, delineated in yellow, indicating that the matrix is polycrystalline. (D and E) STEM-EDS data of REE-bearing monazite grains present in the lamella.

efficiency of recovery of REEs, economics, and environmental impact. Recent studies[36−38] focused on low-temperature coal residues corroborate this trend, showing that the generated ashes possess a lower content of amorphous phases while enabling greater recoveries of REEs. Further work is required, however, to clarify the conditions that enable ash matrices to retain crystallinity while maintaining the large surface area availability required to directly access the REE-bearing minerals.

Lastly, although not the focus of this paper, we present nanoscale structural characterization of REE-bearing minerals in the porous lamella (Figure 3D). TEM and STEM-EDS data

show that the REE-bearing minerals in the porous matrix consist of REE phosphate (i.e., monazite) crystals (Figure 3E and Figure S8). TEM analysis of this study showed that the monazite is comprised of nanosized (∼100 nm) grains rather than one single mineral, suggesting that multiple monazite grains nucleated but failed to grow into a single crystal,[39] or that heat-induced fragmentation of the original single grain occurred.[28] The presence of multiple nanosized REE grains corroborates previous work, indicating that REE-bearing minerals may occur at the nanometer scale and suggest greater surface availability for dissolution reactions. It is also important to note that while other REE mineral phases occur in this

sample,[22] their nanoscale characterization was not pursued in this work given the small volume of investigation of TEM methods.

3.3. Environmental Implications. Coal fly ash is uniquely positioned to serve as a sustainable source of REEs and to reduce the environmental footprint associated with conventional mining. Specifically, repurposing ash for the recovery of REEs creates the opportunity to move the mining industry toward a circular economy, transforming waste products into value-generating assets and sparing virgin mining locations. Adding coal ash to the supply chain of REEs will, however, require the development of extraction processes that are efficient and produce low levels of chemical waste.

This study highlights how the crystallographic structure of REE-hosting ash particles can play an important role in the release of REEs and secondary cations from fly ash. Specifically, dense aluminosilicate particles are composed of amorphous matrices that, although they may assist the transport of reagents and subsequent release of REEs, require reagent-intensive treatments and are expected to release contaminant metals. Crystalline porous particles, in contrast, possess less reactive matrices and, consequently, are expected to enable the recovery of REEs with lower levels of reagent consumption in secondary reactions. Future studies should focus on evaluating additional fluid and solid properties relevant to extraction, including the role of wettability in surface availability for reactions. Additionally, the impact of crystallinity on the effectiveness of alkaline pretreatments, capable of breaking down Si–O bonds, should be further probed. Such efforts, along with the results presented here, are expected to inform the design of more efficient REE extraction methods.

■ ASSOCIATED CONTENT

Sı Supporting Information

The Supporting Information is available free of charge at https://pubs.acs.org/doi/10.1021/acs.estlett.3c00383.

> Summary of the characteristics of the ash sample used in this study (Table S1), BSE micrographs of the particles from which TEM lamellae were extracted (Figure S1), STEM-EDS data collected from the porous lamella (Figure S2), HRTEM micrographs of the porous polycrystalline lamella, including magnified images of crystallites and respective FFT data (Figures S3–S5), *d* spacing frequency analysis for crystal nanograins observed in the porous polycrystalline matrix (Figure S6), ADF-STEM micrographs of the porous lamella (Figure S7), and ADF-STEM and EDS data of REE-bearing monazites found in the porous lamella (Figure S8) (PDF)

■ AUTHOR INFORMATION

Corresponding Author

Wen Song − *Center for Subsurface Energy and the Environment, The University of Texas at Austin, Austin, Texas 78712, United States; Texas Materials Institute, The University of Texas at Austin, Austin, Texas 78712, United States;* ⦿ orcid.org/0000-0003-1913-4503; Phone: (512) 471-5789; Email: wensong@utexas.edu

Authors

Sheila Gerardo − *Center for Subsurface Energy and the Environment, The University of Texas at Austin, Austin, Texas 78712, United States*

Kevin Matthews − *Texas Materials Institute, The University of Texas at Austin, Austin, Texas 78712, United States;* ⦿ orcid.org/0000-0002-4995-2489

Jamie Warner − *Texas Materials Institute, The University of Texas at Austin, Austin, Texas 78712, United States;* ⦿ orcid.org/0000-0002-1271-2019

Complete contact information is available at:
https://pubs.acs.org/10.1021/acs.estlett.3c00383

Notes

The authors declare no competing financial interest.

■ REFERENCES

(1) Vidal, O.; Goffé, B.; Arndt, N. Metals for a Low-Carbon Society. *Nature Geoscience* **2013**, *6*, 894−896.

(2) Alonso, E.; Sherman, A. M.; Wallington, T. J.; Everson, M. P.; Field, F. R.; Roth, R.; Kirchain, R. E. Evaluating Rare Earth Element Availability: A Case with Revolutionary Demand from Clean Technologies. *Environ. Sci. Technol.* **2012**, *46* (6), 3406−3414.

(3) Lacal-Arantegui, R. Materials Use in Electricity Generators in Wind Turbines - State-of-the-Art and Future Specifications. *Journal of Cleaner Production* **2015**, *87* (1), 275−283.

(4) Schmid, M. Challenges to the European Automotive Industry in Securing Critical Raw Materials for Electric Mobility: The Case of Rare Earths. *Mineralogical Magazine* **2020**, *84* (1), 5−17.

(5) Hossain, M. K.; Raihan, G. A.; Akbar, M. A.; Kabir Rubel, M. H.; Ahmed, M. H.; Khan, M. I.; Hossain, S.; Sen, S. K.; Jalal, M. I. E.; El-Denglawey, A. Current Applications and Future Potential of Rare Earth Oxides in Sustainable Nuclear, Radiation, and Energy Devices: A Review. *ACS Applied Electronic Materials* **2022**, *4* (7), 3327−3353.

(6) Zaimes, G. G.; Hubler, B. J.; Wang, S.; Khanna, V. Environmental Life Cycle Perspective on Rare Earth Oxide Production. *ACS Sustainable Chem. Eng.* **2015**, *3* (2), 237−244.

(7) Elshkaki, A. Sustainability of Emerging Energy and Transportation Technologies Is Impacted by the Coexistence of Minerals in Nature. *Nature Communications Earth and Environment* **2021**, *2*, 186.

(8) Xu, Z.; Yang, J.; Zhao, Y.; Hao, R.; Zhang, G. lin. Soil Acidification in a Tailing Area of Ionic Rare Earth in Southeast China. *Sci. Total Environ.* **2023**, *884*, 163834.

(9) Weng, Z. H.; Jowitt, S. M.; Mudd, G. M.; Haque, N. Assessing Rare Earth Element Mineral Deposit Types and Links to Environmental Impacts. *Applied Earth Science* **2013**, *122* (2), 83−96.

(10) Azadi, M.; Northey, S. A.; Ali, S. H.; Edraki, M. Transparency on Greenhouse Gas Emissions from Mining to Enable Climate Change Mitigation. *Nature Geoscience* **2020**, *13* (2), 100−104.

(11) Mardon, S. M.; Hower, J. C. Impact of Coal Properties on Coal Combustion By-Product Quality: Examples from a Kentucky Power Plant. *International Journal of Coal Geology* **2004**, *59*, 153−169.

(12) Taggart, R. K.; Hower, J. C.; Dwyer, G. S.; Hsu-Kim, H. Trends in the Rare Earth Element Content of U.S.-Based Coal Combustion Fly Ashes. *Environ. Sci. Technol.* **2016**, *50* (11), 5919−5926.

(13) Brandt, J. E.; Lauer, N. E.; Vengosh, A.; Bernhardt, E. S.; Di Giulio, R. T. Strontium Isotope Ratios in Fish Otoliths as Biogenic Tracers of Coal Combustion Residual Inputs to Freshwater Ecosystems. *Environmental Science & Technology Letters* **2018**, *5* (12), 718−723.

(14) Wang, Z.; Dwyer, G. S.; Coleman, D. S.; Vengosh, A. Lead Isotopes as a New Tracer for Detecting Coal Fly Ash in the

Environment. *Environmental Science & Technology Letters* **2019**, *6* (12), 714−719.

(15) King, J. F.; Taggart, R. K.; Smith, R. C.; Hower, J. C.; Hsu-Kim, H. Aqueous Acid and Alkaline Extraction of Rare Earth Elements from Coal Combustion Ash. *International Journal of Coal Geology* **2018**, *195*, 75−83.

(16) Pan, J.; Hassas, B. V.; Rezaee, M.; Zhou, C.; Pisupati, S. V. Recovery of Rare Earth Elements from Coal Fly Ash through Sequential Chemical Roasting, Water Leaching, and Acid Leaching Processes. *Journal of Cleaner Production* **2021**, *284*, 124725.

(17) Liu, P.; Huang, R.; Tang, Y. Comprehensive Understandings of Rare Earth Element (REE) Speciation in Coal Fly Ashes and Implication for REE Extractability. *Environ. Sci. Technol.* **2019**, *53* (9), 5369−5377.

(18) Kolker, A.; Scott, C.; Hower, J. C.; Vazquez, J. A.; Lopano, C. L.; Dai, S. Distribution of Rare Earth Elements in Coal Combustion Fly Ash, Determined by SHRIMP-RG Ion Microprobe. *International Journal of Coal Geology* **2017**, *184*, 1−10.

(19) Montross, S. N.; Verba, C. A.; Chan, H. L.; Lopano, C. Advanced Characterization of Rare Earth Element Minerals in Coal Utilization Byproducts Using Multimodal Image Analysis. *International Journal of Coal Geology* **2018**, *195*, 362−372.

(20) Thompson, R. L.; Bank, T.; Montross, S.; Roth, E.; Howard, B.; Verba, C.; Granite, E. Analysis of Rare Earth Elements in Coal Fly Ash Using Laser Ablation Inductively Coupled Plasma Mass Spectrometry and Scanning Electron Microscopy. *Spectrochimica Acta Part B Atomic Spectroscopy* **2018**, *143*, 1−11.

(21) Taggart, R. K.; Rivera, N. A.; Levard, C.; Ambrosi, J. P.; Borschneck, D.; Hower, J. C.; Hsu-Kim, H. Differences in Bulk and Microscale Yttrium Speciation in Coal Combustion Fly Ash. *Environmental Science Processes & Impacts* **2018**, *20* (10), 1390−1403.

(22) Gerardo, S.; Davletshin, A. R.; Loewy, S. L.; Song, W. From Ashes to Riches: Microscale Phenomena Controlling Rare Earths Recovery from Coal Fly Ash. *Environ. Sci. Technol.* **2022**, *56* (22), 16200−16208.

(23) Perez, A.; Daval, D.; Fournier, M.; Vital, M.; Delaye, J. M.; Gin, S. Comparing the Reactivity of Glasses with Their Crystalline Equivalents: The Case Study of Plagioclase Feldspar. *Geochim. Cosmochim. Acta* **2019**, *254*, 122−141.

(24) Hamilton, J. P.; Pantano, C. G.; Brantley, S. L. Dissolution of Albite Glass and Crystal. *Geochim. Cosmochim. Acta* **2000**, *64* (15), 2603−2615.

(25) Cagnon, B.; Daval, D.; Cabié, M.; Lemarchand, D.; Gin, S. A Comparative Study of the Dissolution Mechanisms of Amorphous and Crystalline Feldspars at Acidic PH Conditions. *npj Materials Degradation* **2022**, *6*, 1−13.

(26) Pan, J.; Zhou, C.; Tang, M.; Cao, S.; Liu, C.; Zhang, N.; Wen, M.; Luo, Y.; Hu, T.; Ji, W. Study on the Modes of Occurrence of Rare Earth Elements in Coal Fly Ash by Statistics and a Sequential Chemical Extraction Procedure. *Fuel* **2019**, *237*, 555−565.

(27) Hower, J. C.; Berti, D.; Winkler, C. R.; Qian, D.; Briot, N. J. High-Resolution Transmission Electron Microscopy Study of a Powder River Basin Coal-Derived Fly Ash. *Minerals* **2022**, *12* (8), 975.

(28) Hood, M. M.; Taggart, R. K.; Smith, R. C.; Hsu-Kim, H.; Henke, K. R.; Graham, U.; Groppo, J. G.; Unrine, J. M.; Hower, J. C. Rare Earth Element Distribution in Fly Ash Derived from the Fire Clay Coal, Kentucky. *Coal Combustion and Gasification Products* **2017**, *9* (1), 22−33.

(29) Rasmussen, D.; Carter, C. On the Fresnel Fringe Technique for the Analysis of Interfacial Films. *Ultramicroscopy* **1990**, *32* (4), 337−348.

(30) Shelby, J. E. *Introduction to Glass Science and Technology*, 2nd ed.; Royal Society of Chemistry: Cambridge, U.K., 2005; pp 72−93.

(31) Hemmings, R. T.; Berry, E. E. On the Glass in Coal Fly Ashes: Recent Advances. *Mater. Res. Soc. Symp. Proc.* **1987**, *113*, 3−38.

(32) Shelby, J. E. *Introduction to Glass Science and Technology*, 2nd ed.; Royal Society of Chemistry: Cambridge, U.K., 2005; pp 166−169.

(33) Srinivasachar, S.; Helble, J. J.; Boni, A. A.; Shah, N.; Huffman, G. P.; Huggins, F. E. Mineral Behavior During Coal Combustion 2. Illite Transformations. *Prog. Energy Combust. Sci.* **1990**, *16* (4), 293−302.

(34) Shao, P.; Hou, H.; Wang, W.; Wang, W. Geochemistry and Mineralogy of Fly Ash from the High-Alumina Coal, Datong Coalfield, Shanxi, China. *Ore Geology Reviews* **2023**, *158*, 105476.

(35) Tian, S.; Zhuo, Y.; Chen, C. Characterization of the Products of the Clay Mineral Thermal Reactions during Pulverization Coal Combustion in Order to Study the Coal Slagging Propensity. *Energy Fuels* **2011**, *25* (11), 4896−4905.

(36) Honaker, R. Q.; Zhang, W.; Werner, J. Acid Leaching of Rare Earth Elements from Coal and Coal Ash: Implications for Using Fluidized Bed Combustion to Assist in the Recovery of Critical Materials. *Energy Fuels* **2019**, *33* (7), 5971−5980.

(37) Lin, R.; Soong, Y.; Howard, B. H.; Keller, M. J.; Roth, E. A.; Wang, P.; Granite, E. J. Leaching of Lanthanide and Yttrium from a Central Appalachian Coal and the Ashes Obtained at 550−950 °C. *Journal of Rare Earths* **2022**, *40* (5), 807−814.

(38) Zhang, W.; Honaker, R. Calcination Pretreatment Effects on Acid Leaching Characteristics of Rare Earth Elements from Middlings and Coarse Refuse Material Associated with a Bituminous Coal Source. *Fuel* **2019**, *249*, 130−145.

(39) Brantley, S.; Kubicki, J.; White, A. *Kinetics of Water-Rock Interaction*, 1st ed.; Springer: New York, 2008; pp 259−333.